THE JOURNAL OF PHYSICAL CHEMISTRY C

Article

pubs.acs.org/JPCC

Probing Polymer–Pendant Interactions in the Conducting Redox Polymer Poly(pyrrol-3-ylhydroquinone)

Christoffer Karlsson,[†] Hao Huang,[†] Maria Strømme,[†] Adolf Gogoll,[‡] and Martin Sjödin*[,†]

[†]Nanotechnology and Functional Materials, Department of Engineering Sciences, The Ångström Laboratory, Uppsala University, Box 534, SE-751 21 Uppsala, Sweden

[‡]Department of Chemistry - BMC, Biomedical Centre, Uppsala University, Box 576, SE-751 23 Uppsala, Sweden

Supporting Information

ABSTRACT: Conducting polymers with redox active pendant groups show properties typical of both conducting polymers (i.e., capacitive charging and intrinsic conductivity) and redox polymers (i.e., electrochemical surface response at the formal potential of the pendant groups). The two components can also exert significant interaction on each other during their separate electrochemical reactions. In poly(pyrrol-3-ylhydroquinone), a polypyrrole derivative functionalized with hydroquinone units, the redox conversion of the pendant groups has a large impact on the polymer backbone. This interaction is manifested by a loss of bipolaron states during the hydroquinone oxidation, leading to a decreasing p-doping level with increasing potential, something which, to the best of our knowledge, has never been observed for a conducting polymer. Another effect is a contraction of the polymer film, and subsequent mass loss due to solvent expulsion upon hydroquinone oxidation, which counteracts the normal swelling of polypyrrole with increased potential. The conducting redox polymer under investigation has been synthesized via two routes, leading to different fractions of subunits bearing redox active hydroquinone groups. While the redox potentials are unaffected by the synthesis route, the backbone/pendant group interaction varies notably depending on the degree of quinone functionalization. This type of polymers could find use in, e.g., organic energy storage materials, since the polymer backbone both increases the electronic conductivity and prevents dissolution of the active material, as well as in actuator application, due to polymer contraction over the relatively narrow potential region where the pendant group redox chemistry occurs.

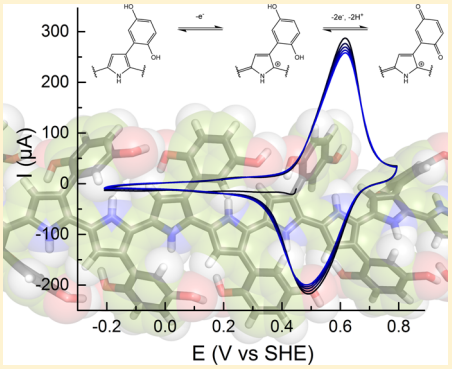

1. INTRODUCTION

Conducting polymers (CPs), by themselves, offer a unique set of properties including potential dependent electronic conductivity[1] and expansion/contraction,[2] as well as electrochromism,[3] electroluminescence,[4] mechanical flexibility,[5] large scale processability,[6] and manufacturing at low temperature and low cost.[6] Since their discovery, CPs have therefore attracted attention in a wide range of applications including actuators, light emitting diodes, displays, molecular electronic components, solar cells, bioelectronics,[7,8] and electrical energy storage.[6,9,10] By attaching functional groups to the CP backbone, additional functionality can be realized.[11−15] The inclusion of such functional groups can, in addition to yielding new material properties, also alter the properties of the CP backbone, through interaction between the functional groups and the backbone.[11,13] Such interaction can either be beneficial or detrimental to the system properties, and knowledge of the design principles governing the interaction is therefore of great value.

In the construction of CP based batteries, a functional group that is redox active can be introduced as a charge storage capacity additive.[13,16−19] This type of polymer, composed of an intrinsically conducting polymer base, with attached redox active pendant groups, will herein be referred to as *conducting redox polymers*. In this case, the polymer backbone serves two purposes: First, it makes the material electronically conducting, owing to the intrinsic bipolaron conductivity of the backbone, and second, it reduces the solubility of the capacity carrying functional group. The polymer backbone also gives the material its mechanical and structural properties. Since the separate advantages of both the functional group (well-defined redox conversion and stability) and of the CP (high conductivity) are desirable for electrode materials in energy storage devices, the material should be designed to keep the independent properties of the polymer base and the redox moiety, while also ensuring fast electron transfer between the two units.

In this report, we investigate the interaction between pendant group and polymer backbone in a conducting redox polymer with hydroquinone redox active functional groups and a polypyrrole (PPy) backbone. A few CPs with quinone pendant groups have previously been reported in the literature,[20] most often with large substituents such as anthraquinone, and often

Received: July 9, 2014
Revised: September 19, 2014
Published: September 22, 2014

   dx.doi.org/10.1021/jp506821z | J. Phys. Chem. C 2014, 118, 23499−23508

Scheme 1. Polymerization and Deprotection of 1 and Polymerization of 2[a]

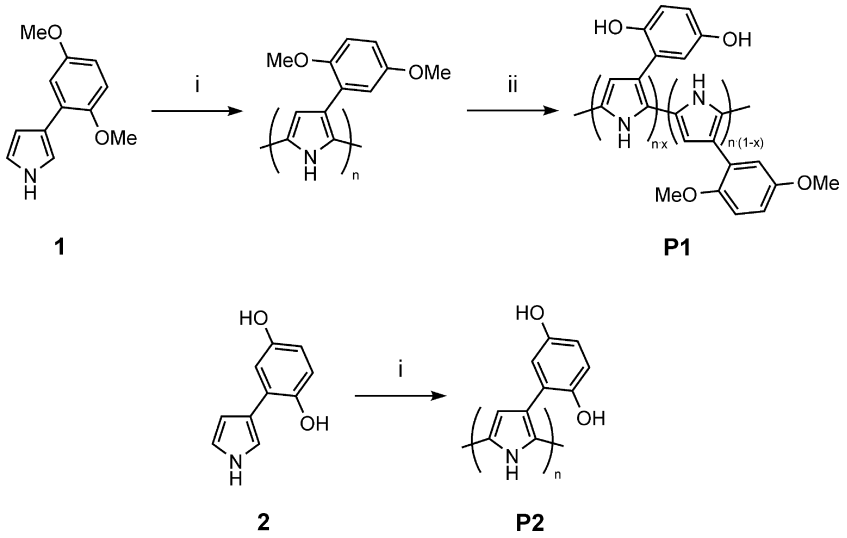

[a] *n* denotes the degree of polymerization, and *x* denotes the degree of quinone functionalization, i.e., the conversion of the deprotection reaction. (i) Polymerization by CV (TBAHFP in MeCN, see Figure 1a); (ii) partial demethylation, BBr_3 (DCM).

attached to PPy on the nitrogen.[21−23] A few polymers have been reported in which hydroquinone pendant groups are attached covalently to PPy, either directly to the backbone[13,19,24] or via aliphatic linkers.[21,25−27] In all of those cases, however, the hydroquinone moieties were diluted with inactive monomeric units, and the properties of those polymers were not studied in great detail. Previous studies of PPy functionalized with hydroquinone pendant groups have relied on polymerization of protected monomers and subsequent deprotection of the formed polymers.[13,25] For example, pyrrol-3-yl-*p*-dimethoxybenzene (**1**) has been polymerized and deprotected to form **P1** (Scheme 1).[13] This results in a degree of quinone functionalization that is less than 100%, and that varies markedly. We herein report the successful synthesis of the monomer pyrrol-3-ylhydroquinone (**2**), which forms a polymer (**P2**) that is similar to **P1** but with close to 100% of monomer units bearing an active hydroquinone pendant group (Scheme 1), and we have investigated the influence of the degree of pendant group functionalization on the properties of the polymer. Spectroelectrochemical measurements show that the polymer doping process stops, or even reverses, during the pendant group redox conversion. Furthermore, large reversible mass changes are observed in a narrow potential interval during the pendant group redox conversion, and the underlying reason for these effects is discussed.

2. EXPERIMENTAL SECTION

All reagents were purchased from Sigma-Aldrich except boronic acid (purchased from Frontier Scientific Inc., purity was determined by NMR to be 75%) and were used without further purification. Tetrahydrofuran (THF) and toluene were dried using a PureSolv PS-MD-4-EN solvent purification system and stored under an argon atmosphere. Flash chromatography was performed using VWR Normasil 60 silica gel (40−63 μm, 60 Å). Analytical thin layer chromatography (TLC) was performed using precoated Merck Silica 60 F254 plates, and compound visualization was achieved with UV light (254 nm). NMR spectra were recorded on a Varian INOVA (^{1}H at 499.93 MHz, ^{13}C at 125.71 MHz) spectrometer. Chemical shifts are reported using the chloroform or acetone solvent signal as an indirect reference to TMS (in *d*-chloroform: δ_H = 7.26 ppm, δ_C = 77.00 ppm; in *d*-acetone: δ_H = 2.05 ppm, δ_C = 206.3 ppm). Coupling constants (*J*) are reported in Hz. IR spectra were recorded for neat compounds on a PerkinElmer Spectrum 100 FT-IR spectrometer with UATR accessory. Mass spectra were recorded on a Thermo Finnigan GCQ mass spectrometer with a direct inlet interface and electron ionization (70 eV). UV/vis spectra were recorded on an Agilent 8453 (for spectroelectrochemical measurements) or a Varian Cary 3 Bio UV/vis spectrophotometer. HRMS was acquired using a Thermo Scientific LTQ Orbitrap Velos apparatus in infusion mode. NMR, IR, UV, and mass spectra can be found in the Supporting Information (Figures S1−S10), as can computational experimental details.

2.1. Monomer Synthesis. The monomer **2** was synthesized with the same strategy as **1**, which has been reported previously (Scheme 2), i.e., Suzuki coupling followed by removal of the tri*iso*propylsilyl (TIPS) protecting group.[13]

Scheme 2. Synthesis Route for 2[a]

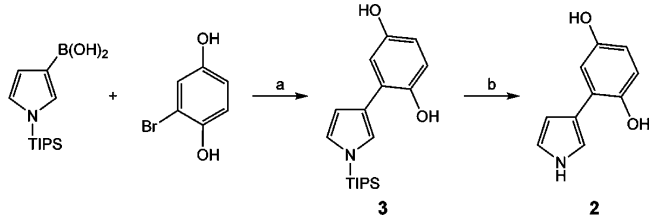

[a] (a) $Pd(PPh_3)_4$, Na_2CO_3, toluene, H_2O; (b) TBAF, THF, AcOH.

*2.1.1. 2-(1-Triisopropylsilylpyrrol-3-yl)-1,4-hydroquinone (**3**).* 1-(Tri*iso*propylsilyl)pyrrol-3-ylboronic acid (0.67 g, 1.9 mmol), 1-bromo-2,5-hydroquinone (0.3 g, 1.6 mmol), and $Pd(PPh_3)_4$ (0.092 g, 0.08 mmol) were dissolved in a toluene/MeOH mixture (8 mL, 1:1 v/v) that was prepurged with argon in a heavy-wall Smith process vial, and then, Na_2CO_3 (2.0 M aq, 0.64 mL, 1.2 mmol) was added. The resulting solution was stirred under argon at 110 °C for 4 h in a microwave cavity. After the reaction finished, the reaction mixture was poured

dx.doi.org/10.1021/jp506821z | J. Phys. Chem. C 2014, 118, 23499−23508

into ice−water (20 mL) and extracted with ethyl acetate (EtOAc). The combined organic phases were washed with brine and dried over $MgSO_4$. The solvent was evaporated under reduced pressure, and a black crude oil was obtained. The crude product was purified on a silica column using gradient eluent (5−50% EtOAc in pentane, v/v). Pure product **3** (0.38 g, 1.1 mmol, 72%) was obtained as a purple solid. ^{1}H NMR (500 MHz, $CDCl_3$): δ_H = 7.01 (1H, dd, J = 2.2, 1.5, Py-H-2), 6.89 (1H, dd, J = 2.7, 2.2, Py-H-5), 6.85 (1H, d, J = 3.1, Ph-H-3), 6.81 (1H, d, J = 8.7, Ph-H-6), 6.63 (1H, dd, J = 8.7, 3.1, Ph-H-5), 6.49 (1H, dd, J = 2.7, 1.5, Py-H-4), 5.30 (1H, bs, OH), 4.56 (1H, bs, OH), 1.48 (3H, sep, J = 7.2, TIPS-CH), 1.13 (18H, d, J = 7.2, TIPS-CH_3) ppm. ^{13}C NMR (125 MHz, $CDCl_3$): δ_C = 149.1, 146.6, 125.8, 123.7, 122.5, 121.4, 115.9, 115.6, 114.0, 110.1, 17.8, 11.6 ppm. mp 116−118 °C. IR (neat): 3284, 2945, 2891, 2866 cm^{-1}. UV/vis (MeOH; λ_{max}): 260, 313, 493 nm. MS (EI; m/z): 331 (100). HRMS (ESI; m/z, $[M + H]^+$): Calcd for $C_{19}H_{30}NO_2Si$, 332.2040; found, 332.2021.

2.1.2. 2-(1-H-Pyrrol-3-yl)-1,4-hydroquinone (2). A 1 mL portion of acetic acid (AcOH) was added to a solution of **3** (0.74 g, 2.2 mmol) in THF (15 mL), followed by addition of a 1.0 M solution of tetra-*n*-butylammonium fluoride (TBAF) in THF (2.2 mL, 2.2 mmol). The reaction mixture was stirred at room temperature for 1 h, and the reaction was monitored by TLC. Precipitation was observed during the reaction. Solvent was removed under reduced pressure, and purple powder was obtained. Crude product was recrystallized from acetone and *n*-heptane, which yielded purple crystals. The product was dissolved in EtOAc and then washed with 0.25 M sodium acetate solution (10 mL) and water (3 × 10 mL). The aqueous phase was re-extracted with EtOAc (3 × 30 mL), and then, the combined organic layers were washed with brine (3 × 30 mL), dried over $NaSO_4$, and concentrated under reduced pressure to give pure **2** (0.27 g, 1.54 mmol, 70%) as brown sticky oil. ^{1}H NMR (500 MHz, $(CD_3)_2CO$): δ_H = 10.04 (1H, bs, NH), 7.56 (2H, bs, OH), 7.42 (1H, m, Py-H-2), 7.02 (1H, d, J = 2.8, Ph-H-3), 6.79 (1H, m, Py-H-5), 6.72 (1H, d, J = 8.4, Ph-H-6), 6.50 (1H, m, Py-H-4), 6.48 (1H, dd, J = 2.8, 8.4, Ph-H-5) ppm. ^{13}C NMR (125 MHz, $(CD_3)_2CO$): δ_C = 150.9, 147.3, 124.6, 120.8, 118.6, 118.1, 116.8, 114.4, 112.6, 107.3 ppm. IR (neat): 3374 cm^{-1}. UV/vis (MeOH; λ_{max}): 260, 312, 473 nm. MS (EI; m/z): 175 (100). HRMS (ESI; m/z, $[M + H]^+$): Calcd for $C_{10}H_{10}NO_2$, 176.0706; found, 176.0697.

2.2. Electrochemistry. An Autolab PGSTAT302N potentiostat (Eco Chemie, The Netherlands) was used for all electrochemical measurements. The organic electrolyte used for polymerization was 0.1 M tetra-*n*-butylammonium hexafluorophosphate (TBAHFP) in dry acetonitrile (MeCN). The aqueous electrolyte consisted of 1.0 M NaCl, $NaNO_3$, or $NaClO_4$, buffered with phosphate, borate, and acetate ions (10 mM each), and the pH was tuned with the respective acid and NaOH (s). All potentials measured in aqueous solutions are reported versus the standard hydrogen electrode (SHE), and all potentials measured in organic solutions are reported versus the ferrocene redox couple ($Fc^{0/+}$). A polished glassy carbon (GC) disk electrode (3.0 mm diameter; BASi, USA) was used as the working electrode, and a Pt wire was used as the counter electrode. In organic solutions, the reference electrode consisted of a Ag wire (10 mM $AgNO_3$, 0.1 M TBAHFP, −0.096 V vs $Fc^{0/+}$) that was kept in a separate compartment. In aqueous solution, a Ag/AgCl reference electrode (3 M NaCl, 0.192 V vs SHE[13]) was immersed directly into the electrolyte solution. The electrolyte was thoroughly degassed with solvent saturated N_2 (g) and kept under N_2 (g) atmosphere throughout the measurements. Electrochemical measurements were performed at room temperature (22 °C).

The charge originating from the quinone redox reaction (Q_Q) was evaluated as the *total* charge in the potential region of the hydroquinone (HQ) to *p*-benzoquinone (Q) redox conversion (close to the formal potential, $E_Q^{0\prime}$), as justified below, and the remaining charge passed in the cyclic voltammetry (CV) experiment was attributed to the PPy backbone capacitive charging (Q_{PPy}). The quinone redox potential was determined from CV measurements, as the average of the oxidation and reduction peak potentials, while the PPy doping onset potential was determined from the maximum slope in the CV.

Redox titration was performed by fixing the potential of the working electrode to 0.447 V vs SHE at pH 1.17 and then increasing the pH by addition of alkaline buffered electrolyte, and recording the potentiostatic current. The cumulative charge at each pH step was recorded, and was compared to the charge passed when incrementally changing the applied potential at pH 1.17. The pH change in the redox titration was correlated to potential change with the conversion factor 59 mV/pH.[13]

2.3. Polymerization. **1** was electropolymerized as reported previously,[13] and **P2** was synthesized in a similar fashion from a 20 mM solution of **2** in organic electrolyte. Polymerization onto a GC electrode was achieved either by CV (−0.5 to +1.0 V vs $Fc^{0/+}$, 0.1 V/s, 5 scans) or potentiostatic chronocoulometry at 0.7 or 0.8 V vs $Fc^{0/+}$ (Scheme 1). The polymer films were washed with EtOH and water to remove residual monomers, short oligomer fragments, and other byproducts from the film.

2.4. Spectroelectrochemistry. **P2** for spectroelectrochemical measurements was electropolymerized onto a working electrode consisting of an indium tin oxide coated quartz slide (8 × 50 × 1 mm^3, 20 Ω/□, Präzisions Glas & Optik, Germany), and the counter electrode was kept in a separate compartment. The conducting substrate was coated with acetate by immersing the glass in a solution of potassium acetate (KOAc, 1.0 M, aq) prior to polymerization.[13] Polymerization was performed by CV as described above but with 10 scans at 20 mV/s, with ∼1 cm^2 immersed in the solution. PPy was synthesized as described previously.[13] The spectroelectrochemical measurements were performed in a quartz cuvette with 1 cm path length, using buffered aqueous electrolyte as described above. CV was performed at 20 mV/s (to ensure negligible *iR* drop), and UV/vis spectra were recorded every 0.5 s. The spectra were correlated with the potential by determining the turning points of the absorbance at 1000 nm, which were assumed to correspond to the CV turning potentials. The derivative of the absorbance with respect to potential (dAbs/dE) was calculated by differentiation and application of a Savitsky−Golay smoothing filter (second order, 20 points).

2.5. Electrochemical Quartz Crystal Microbalance. Electrochemical quartz crystal microbalance (EQCM) measurements were performed using an Autolab potentiostat equipped with a Metrohm EQCM module (Eco Chemie, The Netherlands). The working electrode consisted of a gold coated AT-cut quartz EQCM crystal (6 MHz, 13.6 mm overall diameter, 6.7 mm diameter of the electroactive area), the counter electrode was a Pt wire, and a Ag/AgCl electrode (saturated aqueous KCl gel, 0.173 V vs SHE in water, −0.475 V vs $Fc^{0/+}$ in MeCN) was used as reference. All electrodes were kept directly

dx.doi.org/10.1021/jp506821z | J. Phys. Chem. C 2014, 118, 23499−23508

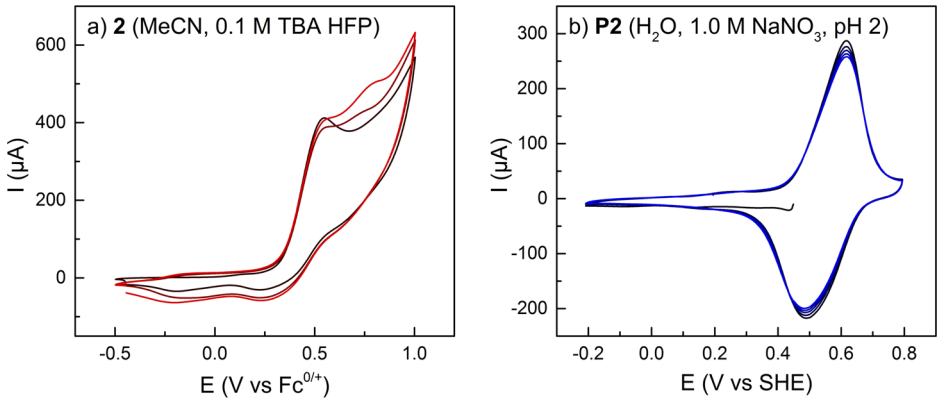

Figure 1. CVs of (a) monomer **2** in organic electrolyte and (b) the polymer **P2** in aqueous electrolyte buffered at pH 2. First scan in black and subsequent scans in lighter color.

in the electrolyte. Polymerization was performed as described above but with either one or five scans, and with a turning potential of 0.63 V vs $Fc^{0/+}$. The aqueous electrolyte was as described above but with only phosphate as buffer. By diluting the 1.0 M electrolytes with water, and then adjusting the pH with the corresponding acid, 0.10 M electrolytes were made. Electrodes covered with polymer were used with different electrolytes, and thorough rinsing with water and new electrolyte was employed between each experiment. In each electrolyte, the polymer was first cycled in a low potential region (below $E_Q^{0'}$) several times to ensure that negligible amounts of other ions were present in the film.

3. RESULTS

3.1. Monomer Synthesis. The synthesis approach toward **2** was based on a method that we have reported previously for the di-*O*-methylated monomer **1**, which uses a Suzuki coupling reaction.[13] 0.8 equiv of Na_2CO_3 were used in this case, rather than the 2 equiv used in the conventional procedure, as it was found to give product **3** in higher yields. Furthermore, in the deprotection step, acetic acid was added to stabilize the hydroquinone unit, which allows the reaction to proceed. Recrystallization gave the tetra-*n*-butylammonium salt of the desired product **3**, which by thorough washing and extraction was converted into the hydroquinone form **3**. It is worth mentioning that, on several occasions, no precipitation occurred during the reaction. In this case, the reaction mixture was worked up without the recrystallization step, which is sufficient to yield the pure product **2**.

3.2. Electrochemical Properties of the Monomer 2. CV of the monomer **2** in MeCN electrolyte (Figure 1a) revealed similar characteristics as those for **1**,[13] namely, an irreversible oxidation peak at 0.5 V vs $Fc^{0/+}$, and large oxidation currents at higher potentials that lead to formation of polymer. When scanning over the latter oxidation, there is a growth of a broad reversible redox feature at low potentials, corresponding to the increasing capacitance of the formed polymer film. Potentiostatic chronocoulometry yielded polymer films with properties comparable to those made by CV polymerization, and allowed for better tuning of the amount of deposited polymer. Potentiostatic chronocoulometry was used for determination of polymerization efficiency (see the Supporting Information for more details), while CV polymerization was used in all other cases.

3.3. Electrochemical Properties of the Polymer P2. **P2** was characterized by CV in aqueous electrolyte buffered at pH 2 (Figure 1b) and exhibits features similar to **P1**:[13] A reversible redox reaction at 0.55 V vs SHE, corresponding to the redox activity of the quinone side chains, and capacitive charging of the PPy backbone, with an onset potential of 0.04 V (Table 1). The quinone peaks are slightly broadened ($E_p - E_{p/2}$ is 83 mV for the oxidation and 91 mV for the reduction) and have a peak split of 101 mV.

Table 1. Summary of P1 and P2 Redox Properties Evaluated from CV Experiments at pH 2

	P1	P2
$E_Q^{0'}$ (V vs SHE)	0.55	0.55
$E_{PPy\ onset}$ (V vs SHE)	0.04	0.04
Q_Q (μC)	444	478
Q_{PPy} (μC)	80	31
Q_{pol} (mC)	15.3	10.6
$Q_Q/(Q_Q + Q_{PPy})$	85%	94%
surface coverage[a] (10^{-8} mol/cm^2)	3.3	3.5

[a]Surface coverage calculated as $\Gamma = Q_Q/zFA$, where $z = 2$, F is the Faraday constant, and A is the electrode area.

The charge originating from the quinone redox conversion and the remaining PPy charge is shown in Table 1 for **P1** and **P2**, together with corresponding surface coverage values. In **P1**, 85% of the total charge capacity is carried by the pendant quinone group, while, in **P2**, almost 94% of the capacity originates from the quinone, indicating significant improvement of the energy storage capacity in **P2**. The quinone charge was also found to be proportional to the charge passed during potentiostatic polymerization (Figure S15, Supporting Information).

Potential steps over the quinone peak yield a sigmoidal charge curve (Figure 2), as expected from the Nernst equation. Fixing the potential of the working electrode below the quinone peak at low pH, and then increasing the pH of the electrolyte to gradually shift $E_Q^{0'}$ below the fixed potential, yields a very similar charge curve as obtained from the potential step measurement (Figure 2), that reaches a plateau value at pH ≈ 7. At higher pH values, degradation charges start to be significant.[28] Since only the quinone potential is affected by the pH change, and not the potential of the PPy backbone (except for the doping state change induced by the quinone oxidation), the total charge measured will be that of the quinone redox conversion. This can then be compared to the charge measured in a CV (Figure 2). For **P2**, the charges during the potential

dx.doi.org/10.1021/jp506821z | J. Phys. Chem. C 2014, 118, 23499−23508

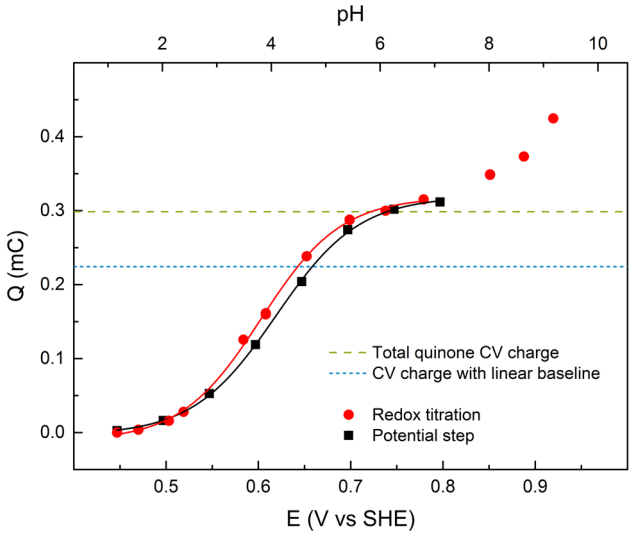

Figure 2. Charge passed during potential step measurements over the quinone peak of **P2** (black squares), during a redox titration (red circles) and in CV at 20 mV/s (dashed vertical lines). Solid lines are fits to the Nernst equation (r^2 = 0.9996 and 0.9990, respectively). The potential and pH *x*-axes are related by 59 mV/pH.

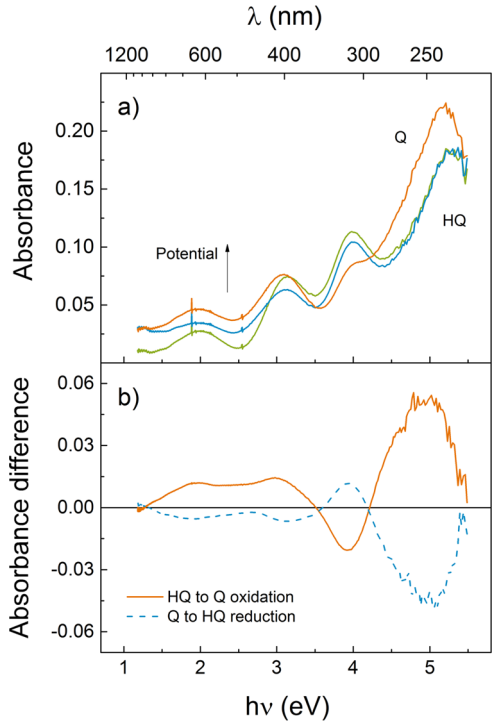

Figure 3. (a) UV/vis/NIR spectra in aqueous electrolyte (1.0 M NaCl at pH 2) for **P2** in the reduced PPy state (green), in the oxidized PPy state (blue), and with oxidized quinone pendant groups (orange). The spectra are recorded at 0.00, 0.37, and 0.72 V vs SHE. (b) Difference spectra over the quinone oxidation (solid orange line) and reduction sweep (dashed blue line) for **P2**, calculated from the same potentials as in part a on the oxidation and reduction sweep. The horizontal axis is the same in parts a and b, with wavelength scale above and energy scale below.

step and redox titration were both 319 μC (the plateau value from the fits to the Nernst equation), which is similar to the total charge in CV (299 μC).

3.4. Spectroelectrochemistry. UV/vis/NIR spectra were recorded on polymer films during *in situ* redox cycling (spectra in Figure 3a, absorbance maxima in Table 2) and were similar to those of **P1** in all redox states. Four absorption bands characteristic of the PPy backbone are present, corresponding to the transitions from the valence band to the midgap states and to the conduction band.[13,29,30] There is also an increase in absorbance at 250 nm coinciding with the HQ to Q redox conversion. Difference spectra (Figure 3b) over this process reveal an additional band assigned to the oxidized Q side groups, and two bands in the reduced HQ state at longer wavelengths. These bands correspond to the quinone centered n–π^* and π–π^* transitions.[13] There were no significant spectral differences upon changing the supporting electrolyte anion from nitrate to chloride or perchlorate.

The absorbances at 250 nm (Abs_{250nm}) and 1000 nm (Abs_{1000nm}) were monitored during redox cycling of **P2** (Figure 4). There is a sigmoidal increase of Abs_{250nm} during the oxidation of the pendant groups that follows a Nernstian behavior. The concentration of bipolaron states on the polymer backbone affects Abs_{1000nm}, which increases linearly for **P2** in the potential regions where the quinone pendant groups are not redox active, as is the case for **P1**[13] as well as for unsubstituted PPy, in the entire stable potential region. **P2**, however, exhibits a decrease of Abs_{1000nm} upon oxidation of the pendant groups, and $dAbs_{1000nm}/dE$ is thus negative at these potentials. Abs_{1000nm} of **P1** is constant during the pendant group oxidation (Figure 4b), and the different behaviors of the two polymers are discussed below.[13] Abs_{250nm} of **P1** and **P2** was fitted to the Nernst equation, and the inflection points coincide with the minima of $dAbs_{1000\ nm}/dE$ (vertical lines in Figure 4), and also with the oxidation peak potentials (**P2** CV in Figure 1b). The absorbances during a reduction sweep follow the same trends reversibly but shifted to more negative potentials, analogous to the electrochemical response.

Table 2. UV/vis/NIR Absorbance Maxima (nm) of P2 in the Reduced (red) and Oxidized (ox) States and with Reduced (HQ) and Oxidized (Q) Pendant Groups, Ascribed to the Q and PPy Transitions

	Q n–π^*	Q π–π^*	PPy 4	PPy 3	PPy 2	PPy 1
ox Q	250[a]	417[a]	306[b]	400	622	>700
ox HQ	315[a]	~500[a,b]	310	394	622	>700
red			311	394	622	

[a]From difference spectra. [b]Shoulder.

3.5. Electrochemical quartz crystal microbalance. The frequency changes (Δf) measured during an EQCM experiment can be related to mass changes per unit area ($\Delta m/A$) on the electrode with the Sauerbrey equation:[31]

$$\frac{\Delta m}{A} = -\frac{\Delta f}{C_f}$$

where C_f = 81.5 Hz cm^2/μg is the sensitivity factor for the crystal, that was verified by calibration by electrodeposition of silver from a $AgNO_3$ solution (50 mM in 0.5 M HNO_3 (aq)). The change in frequency and mass deposited on the electrode during electropolymerization of **2**, calculated using this equation, can be seen in Figure 5. Above the monomer oxidation onset, mass is deposited by precipitation of polymer at a nearly constant rate. At lower potentials, mass changes due to swelling[32] during PPy redox cycling are clearly visible, and

dx.doi.org/10.1021/jp506821z | J. Phys. Chem. C 2014, 118, 23499–23508

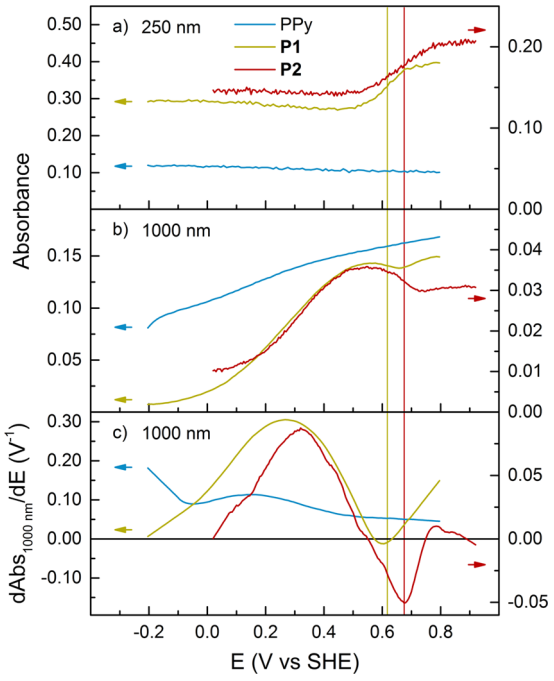

Figure 4. Absorbance traces during a CV oxidation sweep at (a) 250 nm (quinone absorption band) and (b) 1000 nm (PPy band) of unsubstituted PPy (blue, left *y*-axes), **P1** (yellow, left *y*-axes), and **P2** (red, right *y*-axes). (c) Derivative of the absorbance at 1000 nm with respect to potential. Vertical lines indicate the inflection point of the sigmoidal absorbance increase at 250 nm.

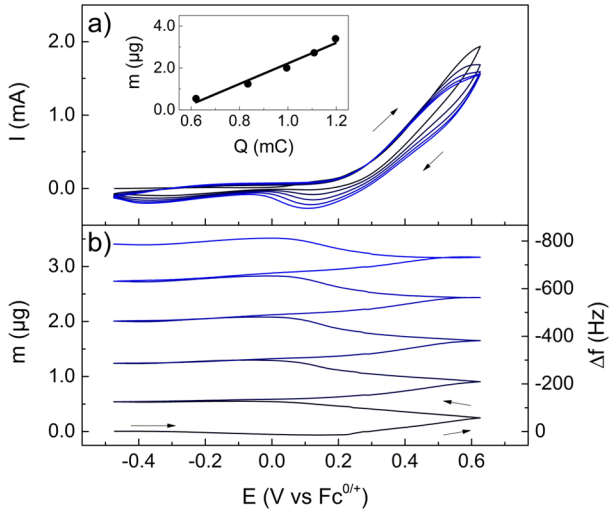

Figure 5. Electropolymerization of **2** onto an EQCM electrode by CV. (a) CV showing polymerization currents and growing **P2** charge. (b) Mass deposited on the electrode during the CV, with the measured frequency change on the right *y*-axis. The inset shows the mass of the neutral polymer vs the capacitive charge of the polymer. The potential scale is the same in parts a and b.

these mass changes increase as more polymer is deposited on the electrode with each sweep. The amount of polymer on the electrode can be determined from the charge passed in a low potential region. Plotting Δf at the low turning potential (corresponding to the mass of the neutral polymer film) versus the capacitive polymer charge (in a low potential interval) reveals a linear relationship (inset in Figure 5), which confirms that Δf can be used to measure the amount of polymer on the electrode.

The mass changes due to anion inclusion and expulsion during PPy oxidation and reduction, respectively, are observed also in aqueous electrolyte ($NaClO_4$ electrolyte in Figure 6,

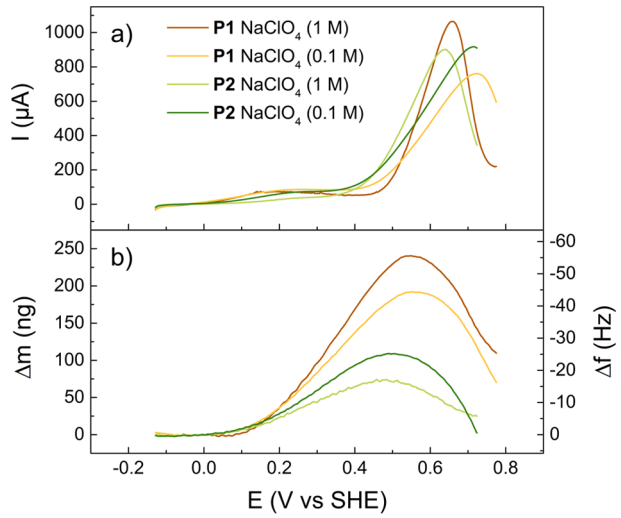

Figure 6. (a) CV oxidation sweep (second scan) of **P1** and **P2** on EQCM electrodes in aqueous electrolyte and (b) the corresponding mass changes, in $NaClO_4$ electrolyte at 1 and 0.1 M, with measured frequency change on the right *y*-axis. The potential scale is the same in parts a and b.

other in Figure S12, Supporting Information). The cumulative charge passed in the CV was evaluated, and the mass was plotted versus the corresponding number of electrons withdrawn from the polymer (*n* in Figure 7b). During the polymer doping process, the mass changes are proportional to the amount of charge passed in the CV (Figure 7b at low *n*) and

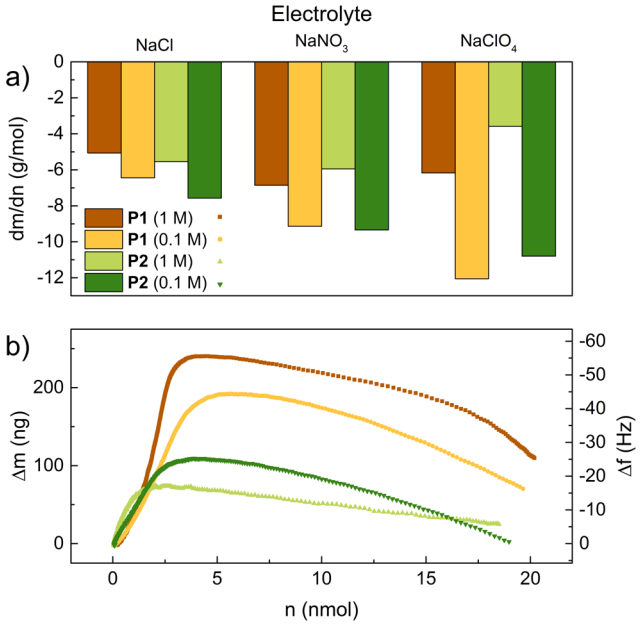

Figure 7. (a) d*m*/d*n* slopes at $E_Q^{0\prime}$ with varying electrolyte and polymer. (b) Mass changes plotted vs the charge passed in CV in $NaClO_4$ electrolyte (same experiment as in Figure 6; measured frequency change on the right *y*-axis).

dx.doi.org/10.1021/jp506821z | J. Phys. Chem. C 2014, 118, 23499−23508

depends on the nature of the supporting electrolyte (Figure S11, Supporting Information). When the pendant groups are oxidized, there is a large mass decrease, on the same order of magnitude as the mass gained upon PPy oxidation (Figure 7b at high n for $NaClO_4$ electrolyte, other in Figure S13, Supporting Information). The mass loss is restored reversibly when the pendant groups are reduced. The slope dm/dn at $E_Q^{0\prime}$ was evaluated (Figure 7a), and a few trends can be observed: (1) There are no significant differences in dm/dn for **P1** and **P2**, but it varies with the electrolyte, and the variation between samples in dm/dn is much greater for **P1** than for **P2**. (2) $|dm/dn|$ is larger for 0.1 M electrolytes than for the corresponding 1 M electrolytes. (3) $|dm/dn|$ is slightly larger for $NaNO_3$ than for NaCl containing electrolytes, but it is smaller for 0.1 M $NaClO_4$ and much larger for 1 M $NaClO_4$. This behavior of the slope is qualitatively related to the polarity of the electrolyte (polarities listed in Table S1, Supporting Information) and not to the molar mass of the electrolyte anion.[33]

4. DISCUSSION

4.1. Monomer Synthesis. The synthesis of **2** was reported in 1992,[24] achieved by deprotection of **1**, but it was later found that the harsh reaction conditions yield impure product,[19] and that deprotection of the monomer is not a viable strategy in this case. Instead, we have successfully employed a route involving Suzuki coupling, which we have previously used to synthesize **1**,[13] with a hydroquinone substrate, to form **3**. Removal of the TIPS group to form the target monomer **2** is readily achieved with slightly different conditions to those used before.[13] The reaction conditions of the Suzuki coupling are currently under further investigation and optimization to achieve the synthesis of other hydroquinone and pyrrole derivatives.

4.2. Monomer Electrochemistry and Polymerization. As observed for **1**,[13] **2** undergoes an irreversible oxidation reaction at 0.5 V vs $Fc^{0/+}$ (Figure 1a), which we have proposed to be centered on the pendant group, rather than on the pyrrole ring. This one electron oxidation leads to formation of the protonated semiquinone state,[15] at the same potential for **1** and **2**.[13] This is expected, since the Hammett *meta* and *para* substituent constants are very similar for OH (0.12 and −0.37) and OMe (0.12 and −0.27).[34] Above 0.6 V, there is a second irreversible oxidation process, centered on the pyrrole moiety, which leads to formation of polymer on the electrode surface. The onset potential for this process is also similar for **1** and **2**, as expected.[13]

4.3. Polymer Electrochemistry. Qualitatively, the electrochemical response of **P2** in aqueous electrolyte is very similar to that of **P1** (Figure 1b).[13] The doping process of the PPy backbone is clearly present, evident as an increase in capacitance at potentials above the doping onset at 0.04 V. This indicates a nondisrupted CP backbone, although the higher onset potential than that for unsubstituted PPy[13] suggests that the pendant groups make the doping process somewhat less favorable. While **P1** and **P2** have similar onset doping potentials, the onset current is less pronounced in **P2** than in **P1** and PPy.[13]

Overlaid on the PPy capacitive response is a reversible redox process at 0.55 V, characteristic of the quinone redox reaction.[13,15,35] The charge of the quinone peak relative to the PPy charge gives a relative estimate of the "degree of quinone functionalization" (the fraction of monomer units bearing a redox active quinone pendant group (x in Scheme 1)), and in **P2**, this is expected to be close to 100%. **P1** is treated with the strong oxidation agent BBr_3 to achieve the deprotected hydroquinone units.[13] The reaction time for this treatment is governed by a trade-off between reaction completion and degrading effects, and the charge capacity carried by the pendant group in this polymer is lower than that in **P2**. Since **P2** is not subjected to BBr_3, it is expected to have a higher conductivity and lower onset doping potential, partly because there is less risk of oxidative degradation and partly because every monomer unit should contain a hydroquinone pendant group, facilitating formation of a more regular polymer structure. It is remarkable that there is no evident difference in the polymer doping onset potential of **P1** and **P2**. This indicates that, under these conditions, the polymer degradation due to BBr_3 is not significant, and that the inherent inhomogeneous nature of **P1** does not affect the PPy conjugation.

4.4. Spectroelectrochemistry. **P1** and **P2** have very similar UV/vis/NIR spectra to unsubstituted PPy in all redox states (Figure 3), which shows that attachment of the pendant groups has little influence on the energetics of the PPy backbone.[13,29,30] The Nernstian increase of the Q absorption band upon oxidation of the pendant groups is clearly visible, and other transitions can be extracted from difference spectra (Figure 3 and Table 2). The most interesting analysis of the spectroelectrochemical data is to compare the evolution of the absorbances at 250 and 1000 nm during an oxidation sweep (Figure 4). Unsubstituted PPy shows only small changes in Abs_{250nm} in the investigated potential range, as do the substituted polymers at potentials sufficiently far from $E_Q^{0\prime}$. Abs_{250nm} can thus be used to uniquely probe the redox state of the pendant groups, since there is a quinone absorption peak at that wavelength (Table 2). As the pendant groups have no absorption band at 1000 nm, where one of the PPy bipolaron absorbance bands is located (transition from the valence band to the lowest midgap level), Abs_{1000nm} can be used to probe the bipolaron concentration in the polymer. For unsubstituted PPy, Abs_{1000nm} increases steadily over the whole potential range, with a slightly higher rate around 0.2 V (where there is also a broad current peak in the CV). The substituted polymers also have the same feature at potentials far from $E_Q^{0\prime}$. However, Abs_{1000nm} reaches a plateau value for **P1** at the hydroquinone oxidation peak potential, indicating a constant bipolaron concentration during the quinone redox process.[13] Intriguingly, Abs_{1000nm} not only levels off but even decreases for **P2** during the pendant group oxidation, which corresponds to a loss of bipolaron states during the hydroquinone oxidation process. These changes can be clearly seen in the derivative of Abs_{1000nm} with potential (Figure 4c). Since degradation processes might occur at high potentials (>0.7 V), we refrain from drawing any conclusions about the absorbance data in this potential region.

The decreasing bipolaron concentration can be interpreted as a reversal of the doping process. To our knowledge, this is the first reported case of decreasing p-doping level with potential in CPs. The reason for the large effects of the pendant group oxidation on the backbone doping level must be that the oxidized form of the pendant groups, Q, increases the energy of the bipolarons on the backbone, compared to the reduced HQ form. Thus, at a certain potential, the polymer is stable at a lower doping level when attached to Q than when attached to HQ units. Considering this, it is not surprising that **P2** exhibits the same effect as **P1** but to a larger degree, since it has a higher degree of quinone functionalization. The origin of this "doping reversal" effect is discussed below.

dx.doi.org/10.1021/jp506821z | J. Phys. Chem. C 2014, 118, 23499−23508

4.5. Separation of Quinone and Polypyrrole Charge Capacity. The recorded current in a CV is the sum of contributions from the PPy backbone, i_{PPy}, and the quinone pendant groups, i_Q ($i = i_{PPy} + i_Q$). A halt of the doping process of **P1** at $E_Q^{0\prime}$ suggests that i_{PPy} decreases to zero at $E_Q^{0\prime}$. For **P2**, in which the doping rate is reversed, i_{PPy} is negative at $E_Q^{0\prime}$ and the polymer backbone thus gives a negative contribution to the total current during the quinone oxidation process. In fact, pH titration shows that, in this polymer, the total charge passed during the pendant group redox conversion in CV experiments is attributed to quinone oxidation (Figure 2). Since the charge is identical whether the redox conversion is brought on by an alteration in quinone formal potential by pH change or by variation in potential, where the polymer backbone could give a charge change and hence give an additional contribution to the total charge passed, the total contribution from the polymer backbone redox conversion must be negligible over the quinone peak. The quinone contribution to the total capacity was therefore evaluated from the total charge under the quinone peak, since a linear baseline for the quinone CV peak would greatly underestimate Q_Q.

4.6. Electrochemical Quartz Crystal Microbalance. EQCM has been extensively used to study the redox reactions in CPs.[32,36,37] Several assumptions are made when using the Sauerbrey equation to correlate the frequency change and mass change, e.g., that the density of the polymer is homogeneous throughout the film and equal to that of quartz, that the thickness of the film is constant over the active area, and that the viscoelasticity of the film does not change during the course of the measurement.[31] These conditions have been shown to generally hold for thin CP films.[36,37] The deposition of mass can be followed during electropolymerization of **2** (Figure 5), and the increase in capacitive polymer charge follows the mass increase as expected. The mass of the neutral polymer varies with the capacitive polymer charge with the slope 4.894 μg/mC, corresponding to 472.2 g/mol, which is the molar mass of the unit in the polymer that can store one charge in the backbone, including MeCN electrolyte. This is in the right order of magnitude (corresponding, e.g., to three pyrrole units, two MeCN molecules, and 1/2 residual TBA HFP ion pair), and the linearity serves to justify using the Sauerbrey equation.

During an oxidation sweep in aqueous electrolyte of an electrode covered with **P2**, the mass changes vary with potential in four regions: (1) at $E < 0.2$ V, where the PPy backbone is reduced and no redox processes occur, the mass is constant, (2) at 0.2 V $< E <$ 0.5 V, i.e., oxidized backbone but far from $E_Q^{0\prime}$, the mass increases linearly (both with respect to potential and the amount of charge passed), (3) close to $E_Q^{0\prime}$, at 0.5 V $< E <$ 0.8 V, the mass decreases approximately linearly with the amount of charge passed (Figures 6 and 7), and (4) at $E > 0.8$ V, where all pendant groups are oxidized, the mass continues to increase linearly. Extensive cycling at the latter high potentials degrades the polymer, however, and that potential region was thus not explored extensively. The same processes occur in reverse during the reduction sweep, but the quinone process is shifted to more negative potentials, following the CV reduction peak. The slope of Δm vs n (dm/dn, where n is the amount of electrons withdrawn in the CV) far from $E_Q^{0\prime}$ corresponds to the effective mass change that the polymer undergoes in the PPy doping process for each mole of charge passed. In most cases, this is less than the molar mass of the negative electrolyte ion, which is likely due to the simultaneous counter flux of cations.[32,38] It should be noted that difficulties in determination of the small currents passed in this potential region will greatly affect dm/dn but that the relative mass changes can still be qualitatively compared.[31]

The most interesting feature of the EQCM measurements is the mass decrease occurring in a relatively narrow potential range close to $E_Q^{0\prime}$ (Figure 6). The mass decrease closely follows the quinone current peak, and a plot of mass versus charge passed in the CV is approximately linear (Figure 7). The slope dm/dn shows large variation between different preparations for **P1** (which is not the case for **P2**), reflecting the unreliability of the demethylation reaction performed on **P1**, yielding a varying degree of quinone functionalization. The mass decrease is much too large to only be an effect of either the loss of HQ protons or the doping reversal seen in the spectroelectrochemical experiments. Moreover, there is no systematic variation in dm/dn with anion molar mass in this potential region, indicating that the reduction of the CP during pendant group oxidation, as evidenced by spectral changes, is a secondary effect induced by the redox chemistry of the pendant group. Furthermore, the dm/dn values of **P2** are comparable to those of **P1**, in which the doping does not reverse but merely halts. Although the dominant dm/dn variation with electrolyte in this potential region is not dependent on the molar mass of the electrolyte ions, it does depend on the electrolyte composition through the solvent polarity (Table S1, Supporting Information). We hypothesize that the decrease in polarity of the pendant groups, as they are oxidized, leads to expulsion of solvent due to the increased free energy of the solvent in the polymer phase as a result of the polarity change. The solvent expulsion could also be an effect of increased intra- and/or interpolymer chain interactions via the pendant group, when going from the HQ to the Q state. While HQ can form hydrogen bonds between PGs and with water, the interaction between the HQ π systems is limited. When oxidized Q units are formed, however, there are possibilities for strong pendant group interaction through HQ−Q interaction (forming stable quinhydrone complexes[39]) and Q−Q interaction, both via $\pi-\pi$ stacking.[40] Such enhanced interaction would cause a contraction of the polymer, forcing solvent out of the polymer structure, and the effect would be larger for more polar electrolytes. $|dm/dn|$ increases slightly with n (Figure S14, Supporting Information), which means that pendant groups that are oxidized at the end of the peak lead to a larger mass decrease (per electron removed), indeed indicating increased interaction in the oxidized form. On the other hand, while this latter model predicts a larger mass change $|dm/dn|$ for polymers with a higher degree of quinone functionalization, there is no significant difference in $|dm/dn|$ between **P1** and **P2** (Figure 7a), which contradicts this model.

4.7. On the Origin of the Bipolaron Loss. The presented spectroelectrochemical results show that, during the HQ to Q redox conversion in **P2**, the polymer backbone absorption, attributed to the bipolaron state, is decreased at $E_Q^{0\prime}$. This clearly indicates that, in this potential interval, either the doping process is reversed or the charges originally present as bipolarons are converted to other species. In the complex polymer system under study, there are several possibilities to account for this interesting feature. The Q units are expected to create a less polar environment than HQ, increasing the energy of all charged species in the polymer, in particular localized charges. The bipolarons thus become destabilized relative to the neutral state, leading to a decreased doping level. In this model, a variation of the electrolyte ions is not expected to lead

dx.doi.org/10.1021/jp506821z | J. Phys. Chem. C 2014, 118, 23499−23508

to different degrees of doping reversal, as the effect is only depending on the polarity of the pendant groups and of the bipolarons, and not that of the solvent. The extra expulsion of electrolyte in more polar solvents (as seen in EQCM) does not therefore lead to more dedoping, which is in agreement with the observed behavior.

In addition to the model described above, there are two other effects that could contribute to the observed properties of **P1** and **P2**, and which cannot be excluded at present. First, as we have previously suggested, the HQ to Q redox conversion could affect the energy of the bipolaron charges inductively, thus destabilizing oxidized polymer states relative to neutral states, upon oxidation of the pendant group.[13] This effect must be predominantly due to induction rather than resonance, however, since the pendant groups are twisted out of the polymer backbone plane due to steric restrictions (Figure 8).

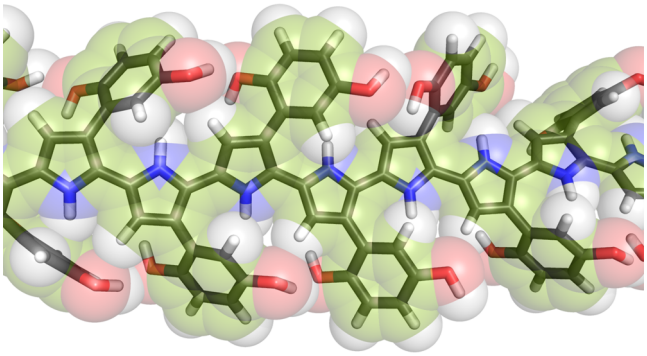

Figure 8. Structure of **P2** in the reduced state (stick model with black carbons and semitransparent van der Waals spheres with green carbons; structure optimized with DFT; see the Supporting Information for computational details). There is very limited space around the backbone to accommodate the bulk of the pendant groups, forcing them to twist out of plane.

Previous computational studies support this model by showing that the Mulliken charge of pyrrole is significantly less when attached to a Q unit compared to when it is attached to HQ.[13] A second alternative that is in good agreement with the presented EQCM data is a model where the Q–Q interaction causes a contraction of the polymer in the oxidized state, thus explaining the mass change seen in EQCM. Packing of nearby quinone units will, by necessity, disrupt the polymer planarity and thus shorten the conjugation length in the polymer backbone (Figure 8). Such twisting of the polymer could also force localization of the charges on the polymer, accounting for the loss of the bipolaron absorption. As shorter polymer segments in general have a higher reduction potential than longer segments, this also leads to a destabilization of the oxidized form of the polymer backbone and a formal reduction of the polymer.[41]

Efforts in our group will continue toward elucidation of the mechanisms responsible for the doping reversal and the mass changes during redox cycling. Specifically, a series of linker units has been introduced between the polymer backbone and the hydroquinone units, and its effect on the interaction between the two moieties is being studied, and will be the focus of future publications. We are also investigating the rate limiting factors of the polymer redox reactions, as well as the *in situ* conductivity, which are important factors in applications such as energy storage and molecular electronics.

5. CONCLUSIONS

A conducting redox polymer with a polypyrrole base and hydroquinone pendant groups has been produced by two synthesis routes—one by demethylation of the *p*-dimethoxyphenyl substituted polymer and one by polymerization of pyrrol-3-ylhydroquinone—and the resulting polymers are compared. While the two polymers show close to identical energetics, i.e., equal polymer doping onset potentials and quinone reduction potentials, as well as similar spectroscopic features, the second synthetic route yields an enhanced degree of quinone functionalization. Both polymers show significant perturbation of the polymer backbone during pendant group redox conversion, i.e., upon oxidation of the pendant group, in the form of a loss of bipolaron states and a mass decrease of the polymer. This is, to our knowledge, the first reported case of a CP that exhibits a reversible decrease in p-doping level with increasing potential. We argue that the doping reversal as well as the mass reduction is due to a polarity change upon pendant group redox conversion that destabilizes the bipolaron state and increases the free energy of the solvent in the polymer, thus causing solvent expulsion and reduction of the polymer.

■ ASSOCIATED CONTENT

Ⓢ Supporting Information

NMR, IR, UV, and mass spectra, EQCM plots, dielectric constants of electrolytes, polymerization efficiency, and computational experimental details. This material is available free of charge via the Internet at http://pubs.acs.org.

■ AUTHOR INFORMATION

Corresponding Author

*Phone: +46 18 471 73 30. E-mail: Martin.Sjodin@Angstrom.uu.se.

Notes

The authors declare no competing financial interest.

■ ACKNOWLEDGMENTS

Bo Ek is gratefully acknowledged for HRMS measurements. The authors would also like to thank the Swedish Foundation for Strategic Research (SSF), The Carl Trygger Foundation, The Swedish Energy Agency (project SweGRIDS), and the European Institute of Innovation and Technology under the KIC InnoEnergy NewMat and electrical energy storage project for their financial support of this work.

■ REFERENCES

(1) Zotti, G.; Zecchin, S.; Schiavon, G.; Berlin, A.; Pagani, G.; Canavesi, A. Conductivity in Redox Modified Conducting Polymers. 2. Enhanced Redox Conductivity in Ferrocene-Substituted Polypyrroles and Polythiophenes. *Chem. Mater.* **1995**, *7*, 2309–2315.

(2) Jager, E. W. H.; Smela, E.; Inganäs, O. Microfabricating Conjugated Polymer Actuators. *Science* **2000**, *290*, 1540–1545.

(3) Dyer, A. L.; Thompson, E. J.; Reynolds, J. R. Completing the Color Palette with Spray-Processable Polymer Electrochromics. *ACS Appl. Mater. Interfaces* **2011**, *3*, 1787–1795.

(4) Matyba, P.; Yamaguchi, H.; Chhowalla, M.; Robinson, N. D.; Edman, L. Flexible and Metal-Free Light-Emitting Electrochemical Cells Based on Graphene and Pedot-Pss as the Electrode Materials. *ACS Nano* **2010**, *5*, 574–580.

(5) Meng, C.; Liu, C.; Chen, L.; Hu, C.; Fan, S. Highly Flexible and All-Solid-State Paperlike Polymer Supercapacitors. *Nano Lett.* **2010**, *10*, 4025–4031.

(6) Song, Z.; Zhou, H. Towards Sustainable and Versatile Energy Storage Devices: An Overview of Organic Electrode Materials. *Energy Environ. Sci.* **2013**, *6*, 2280−2301.
(7) Persson, K. M.; Karlsson, R.; Svennersten, K.; Loffler, S.; Jager, E. W. H.; Richter-Dahlfors, A.; Konradsson, P.; Berggren, M. Electronic Control of Cell Detachment Using a Self-Doped Conducting Polymer. *Adv. Mater.* **2011**, *23*, 4403−4408.
(8) Ferraz, N.; Carlsson, D. O.; Hong, J.; Larsson, R.; Fellström, B.; Nyholm, L.; Strømme, M.; Mihranyan, A. Haemocompatibility and Ion Exchange Capability of Nanocellulose Polypyrrole Membranes Intended for Blood Purification. *J. R. Soc., Interface* **2012**, *9*, 1943−1955.
(9) Miller, J. S. Conducting Polymers—Materials of Commerce. *Adv. Mater.* **1993**, *5*, 671−676.
(10) Nyholm, L.; Nyström, G.; Mihranyan, A.; Strømme, M. Toward Flexible Polymer and Paper-Based Energy Storage Devices. *Adv. Mater.* **2011**, *23*, 3751−3769.
(11) Holliday, B. J.; Swager, T. M. Conducting Metallopolymers: The Roles of Molecular Architecture and Redox Matching. *Chem. Commun.* **2005**, 23−36.
(12) Deronzier, A.; Moutet, J. C. Functionalized Polypyrroles. New Molecular Materials for Electrocatalysis and Related Applications. *Acc. Chem. Res.* **1989**, *22*, 249−255.
(13) Karlsson, C.; Huang, H.; Strømme, M.; Gogoll, A.; Sjödin, M. Polymer−Pendant Interactions in Poly(Pyrrol-3-Ylhydroquinone): A Solution for the Use of Conducting Polymers at Stable Conditions. *J. Phys. Chem. C* **2013**, *117*, 23558−23567.
(14) Karlsson, C.; Jämstorp, E.; Strømme, M.; Sjödin, M. Computational Electrochemistry Study of 16 Isoindole-4,7-Diones as Candidates for Organic Cathode Materials. *J. Phys. Chem. C* **2012**, *116*, 3793−3801.
(15) Karlsson, C.; Gogoll, A.; Strømme, M.; Sjödin, M. Investigation of the Redox Chemistry of Isoindole-4,7-Diones. *J. Phys. Chem. C* **2013**, *117*, 894−901.
(16) Milczarek, G.; Inganäs, O. Renewable Cathode Materials from Biopolymer/Conjugated Polymer Interpenetrating Networks. *Science* **2012**, *335*, 1468−1471.
(17) Rosciano, F.; Salamone, M. M.; Ruffo, R.; Sassi, M.; Beverina, L. Crosslinked Electroactive Polymers Containing Naphthalene-Bisimide Redox Centers for Energy Storage. *J. Electrochem. Soc.* **2013**, *160*, A1094−A1098.
(18) Xu, L. Synthesis and Properties of Novel Tempo-Contained Polypyrrole Derivatives as the Cathode Material of Organic Radical Battery. *Electrochim. Acta* **2014**, *130*, 148−155.
(19) Rose, T. L.; Kon, A. B.; Wang, F. High Charge Storage Conductive Polymer. *Abstr. Pap. Am. Chem. Soc.* **1995**, *209*, 311−312.
(20) Curran, D.; Grimshaw, J.; Perera, S. D. Poly(Pyrrole) as a Support for Electrocatalytic Materials. *Chem. Soc. Rev.* **1991**, *20*, 391−404.
(21) Andrieux, C. P.; Audebert, P. First Electrochemical Study of a Modified Electrode Obtained from a 3-Functionalized Pyrrole Derivative. *J. Electroanal. Chem. Interfacial Electrochem.* **1989**, *261*, 443−448.
(22) Audebert, P.; Bidan, G.; Lapkowski, M. Reduction by Two Successive One-Electron Transfers of Anthraquinone Units Bonded to Electrodeposited Poly(Pyrrole) Films *J. Chem. Soc. Chem. Commun.* **1986**, 887−889.
(23) Grimshaw, J.; Perera, S. D. Redox Behaviour of Polypyrrole Films Containing Naphthoquinone and Benzoquinone Groups. *J. Electroanal. Chem. Interfacial Electrochem.* **1990**, *281*, 125−132.
(24) Kon, A. B.; Foos, J. S.; Rose, T. L. Synthesis and Properties of Poly(3-Hydroquinonylpyrrole). *Chem. Mater.* **1992**, *4*, 416−424.
(25) Foos, J. S.; Degnan, S. M.; Glennon, D. G.; Beebe, X. Polypyrroles Derivatized in the 3-Position with Dimethoxybenzene and Quinone Functionalities. *J. Electrochem. Soc.* **1990**, *137*, 2530−2533.
(26) Aquino-Binag, C. N.; Kumar, N.; Lamb, R. N.; Pigram, P. J. Fabrication and Characterization of a Hydroquinone-Functionalized Polypyrrole Thin-Film Ph Sensor. *Chem. Mater.* **1996**, *8*, 2579−2585.
(27) Inagaki, T.; Hunter, M.; Yang, X. Q.; Skotheim, T. A.; Lee, H. S.; Okamoto, Y. Electrochemical Polymerization of Pyrrole Derivatives. *Mol. Cryst. Liq. Cryst. Incorporating Nonlinear Opt.* **1988**, *160*, 79−88.
(28) Olsson, H.; Nyström, G.; Strømme, M.; Sjödin, M.; Nyholm, L. Cycling Stability and Self-Protective Properties of a Paper-Based Polypyrrole Energy Storage Device. *Electrochem. Commun.* **2011**, *13*, 869−871.
(29) Brédas, J.-L.; Street, G. B. Polarons, Bipolarons, and Solitons in Conducting Polymers. *Acc. Chem. Res.* **1985**, *18*, 309−315.
(30) Čabala, R.; Škarda, J.; Potje-Kamloth, K. Spectroscopic Investigation of Thermal Treatment of Doped Polypyrrole. *Phys. Chem. Chem. Phys.* **2000**, *2*, 3283−3291.
(31) Buttry, D. A.; Ward, M. D. Measurement of Interfacial Processes at Electrode Surfaces with the Electrochemical Quartz Crystal Microbalance. *Chem. Rev.* **1992**, *92*, 1355−1379.
(32) Akieh, M. N.; Price, W. E.; Bobacka, J.; Ivaska, A.; Ralph, S. F. Ion Exchange Behaviour and Charge Compensation Mechanism of Polypyrrole in Electrolytes Containing Mono-, Di- and Trivalent Metal Ions. *Synth. Met.* **2009**, *159*, 2590−2598.
(33) Harris, F. E.; O'Konski, C. T. Dielectric Properties of Aqueous Ionic Solutions at Microwave Frequencies. *J. Phys. Chem.* **1957**, *61*, 310−319.
(34) Hansch, C.; Leo, A.; Taft, R. W. A Survey of Hammett Substituent Constants and Resonance and Field Parameters. *Chem. Rev.* **1991**, *91*, 165−195.
(35) Chambers, J. Q. In *The Chemistry of the Quinonoid Compounds*; Patai, S., Ed.; John Wiley & Sons: London, 1974; Vol. *1*, pp 737−791.
(36) Orata, D.; Buttry, D. A. Determination of Ion Populations and Solvent Content as Functions of Redox State and Ph in Polyaniline. *J. Am. Chem. Soc.* **1987**, *109*, 3574−3581.
(37) Kaufman, J. H.; Kanazawa, K. K.; Street, G. B. Gravimetric Electrochemical Voltage Spectroscopy: In Situ Mass Measurements During Electrochemical Doping of the Conducting Polymer Polypyrrole. *Phys. Rev. Lett.* **1984**, *53*, 2461−2464.
(38) Hepel, M.; Dentrone, L.; Seymour, E. In *Polymer Solutions, Blends, and Interfaces*; Noda, I., Rubingh, D. N., Eds.; Elsevier Science Publ B V: Amsterdam, The Netherlands, 1992; Vol. *11*, pp 385−405.
(39) Hesse, M.; Meier, H.; Zeeh, B. In *Spectroscopic Methods in Organic Chemistry*, 2nd ed.; Georg Thieme Verlag: Stuttgart, Germany, 2008; pp 23−24.
(40) Bernstein, J.; Cohen, M. D.; Leiserowitz, L. In *The Chemistry of the Quinonoid Compounds*; Patai, S., Ed.; John Wiley & Sons: London, 1974; Vol. *1*, pp 37−110.
(41) Heinze, J.; Frontana-Uribe, B. A.; Ludwigs, S. Electrochemistry of Conducting Polymers - Persistent Models and New Concepts. *Chem. Rev.* **2010**, *110*, 4724−4771.